Analytical and Bioanalytical Chemistry (2020) 412:8379–8389
https://doi.org/10.1007/s00216-020-02974-1

RESEARCH PAPER

Water-soluble ZnCuInSe quantum dots for bacterial classification, detection, and imaging

Hongchao Geng[1] · Yan Qiao[1] · Ning Jiang[1] · Chenyi Li[1] · Xingqi Zhu[1] · Weili Li[2] · Qingyun Cai[1]

Received: 22 July 2020 / Revised: 14 September 2020 / Accepted: 24 September 2020 / Published online: 30 September 2020

Abstract

Bacteria are everywhere and pose severe threats to human health and safety. The rapid classification and sensitive detection of bacteria are vital steps of bacterial community research and the treatment of infection. Herein, we developed optical property–superior and heavy metal–free ZnCuInSe quantum dots (QDs) for achieving rapid discrimination of Gram-positive/Gram-negative bacteria by the naked eye; driven by the structural differences of bacteria, ZnCuInSe QDs are effective in binding to Gram-positive bacteria, especially *Staphylococcus aureus* (*S. aureus*), in comparison with Gram-negative bacteria and give discernable color viewed by the naked eye. Meanwhile, based on its distinctive fluorescence response, the accurate quantification of *S. aureus* was investigated with a photoluminescence system in the concentration ranges of 1×10^3 to 1×10^{11} CFU/mL, with a limit of detection of 1×10^3 CFU/mL. Furthermore, we demonstrated the feasibility of ZnCuInSe QDs as a fluorescence probe for imaging *S. aureus*. This simple strategy based on ZnCuInSe QDs provides an unprecedented step for rapid and effective bacterial discrimination, detection, and imaging.

Keywords ZnCuInSe QDs · Bacterial classification · Detection · Imaging

Introduction

Pathogenic bacteria are everywhere and induce harsh threats to human health and safety, causing more than 10 million deaths every year in the world [1, 2]. The effective and rapid classification of bacteria based on the differences in cellular composition or cellular structure is the elementary first step for the effective treatment. Meanwhile, the sensitive detection of bacterial concentrations is also a critical step in clinical diagnosis and food safety [3]. The gold standard for bacterial classification, Gram staining, is quite robust and has been used in various bacteria; however, it requires complicated multistep procedures, causing its accuracy to be low. Also, traditional bacterial detection methods, such as the standard plate count, generally take several days [4]. Although surface plasmon resonance [5–7], surface-enhanced Raman scattering [8–10], enzyme-linked immunosorbent assays [11, 12], and mass spectrometry [13, 14] are commonly used for bacterial detection in the laboratory and these methods are accurate and sensitive, they require expensive, relatively large equipment and professional operators, resulting in poor adaptability for field analysis. Fluorescence is a hopeful visual tool for rapid and reliable identification and detection of bacteria due to its high sensitivity. Meanwhile, the superior fluorescent probe is the basis for bacterial discrimination, detection, and imaging.

Semiconductor quantum dots (QDs) are widely used in the fields of biological sensing [15, 16] due to their high quantum yields (QYs) [17], adjustable emission wavelength range [18], resistance to photobleaching [19], and controllable particle size [20]. For example, Lin and co-workers prepared immunomagnetic beads and CdSe/ZnS core/shell QDs to detect *Escherichia coli* (*E. coli*) O157:H7 as low as 14 CFU/mL within 2 h [21]. Guo et al. developed highly fluorescent CdTe/CdS core/shell QDs as a novel label to conjugate with polyclonal antibodies to rapidly detect *E. coli* O157:H7 [22]. However, these QDs are mainly focused on highly toxic cadmium and lead chalcogenides, which make the future clinical

✉ Weili Li
liweiliziji11@126.com

✉ Qingyun Cai
qycai0001@hnu.edu.cn

[1] State Key Laboratory of Chemo/Biosensing and Chemometrics, College of Chemistry and Chemical Engineering, Hunan University, Changsha 410082, Hunan, China

[2] College of Chemistry and Environmental Engineering, Pingdingshan University, Pingdingshan 467000, Henan, China

application doubtful based on health and environmental issues [23]. As a contrast, less toxic I-III-VI_2 group QDs, notably $CuInSe_2$ QDs, with high absorption coefficients (~ 10^5 cm^{-1}) and direct band gaps of 1.04 eV are more suitable for biological application, receiving widespread attention [24, 25]. Allen and co-workers reported synthesis of $CuInSe_2$ QDs with PL QY up to 25% [26]. Jeaho and co-workers synthesized CuInSe/ZnS core/shell near-infrared QDs for biomedical imaging [27]. Moreover, Zn^{2+} has been introduced into the vacant lattice sites of ternary QDs to improve fluorescence performance due to the reduced density of trapping defects. For example, Deng and co-workers prepared aqueous ZnCuInSe/ZnS QDs via ligand exchange for optical imaging in cells [28]. Pons et al. synthesized near-infrared ZnCuInSe/ZnS QDs for in vivo imaging of tumor cells [29]. In addition, Zn doping is found to improve chemical stability. To the best of our knowledge, ZnCuInSe QDs have not been applied to bacteria research.

In this work, we report a straightforward synthesis strategy to transfer ZnCuInSe QDs from organic to aqueous solvents with good fluorescence performance and tunable emission [30]. The effects of Zn content on the photoluminescence properties and structure of the QDs are investigated. Then, a novel ZnCuInSe QDs–based fluorescence sensor for classification, quantification, and imaging of *Staphylococcus aureus* is presented, as shown in Scheme 1. For classification of bacteria, different surface structures and chemical components of Gram-positive/Gram-negative bacteria determine ZnCuInSe QDs could or not bind to their cell membrane, thus successfully displaying information into fluorescence colors, achieving fast discrimination of them by the naked eye. For *S. aureus* detection, the fluorescence intensity of ZnCuInSe QDs was significantly enhanced due to the formed ZnCuInSe QDs-*S. aureus* complex after the incubation of ZnCuInSe QDs and *S. aureus*. In addition, ZnCuInSe QDs were successfully applied to the imaging of *S. aureus*, demonstrating possible applications of QDs in the biological field.

Experimental section

Chemicals

Zinc chloride (99.9%), copper(I) chloride (99.998%), oleylamine (80–90%), 1-dodecanethiol (98%), 1-octadecene (90%), and 3-mercaptopropionic acid (98%) were obtained from Aladdin (Shanghai, China). L-Glutathione (98%), indium(III) chloride tetrahydrate (99.99%), and Se powder (200 mesh, 99.99%) were purchased from Energy Chemical (Shanghai, China). 4′,6-Diamidino-2-phenylindole (DAPI, 5 mg mL^{-1}) was purchased from Beyotime Institute of Biotechnology (Shanghai, China). All chemicals were used as received without further processing. The Hek293T cells and NIH/3T3 cells were purchased from American Type Culture Collection (ATCC, Manassas, VA, USA). The red blood cells of sheep and the calf serum were obtained from Changsha Bell Biotech Co., Ltd. (Changsha, China).

Synthesis of hydrophobic ZnCuInSe QDs

A series of hydrophobic ZnCuInSe QDs were synthesized by hot-injection method [30]. Typically, 0.1 mmol of zinc chloride, 0.03 mmol of copper(I) chloride, and 0.1 mmol of indium(III) chloride tetrahydrate were placed in a three-neck flask with 3 mL of 1-dodecanethiol, 1 mL of 1-octadecene, and 5 mL of oleylamine. The reaction mixture was degassed under vacuum for 30 min at 30 °C. After that, the mixture was heated to 160 °C with 15 °C min^{-1}. Then, a Se precursor

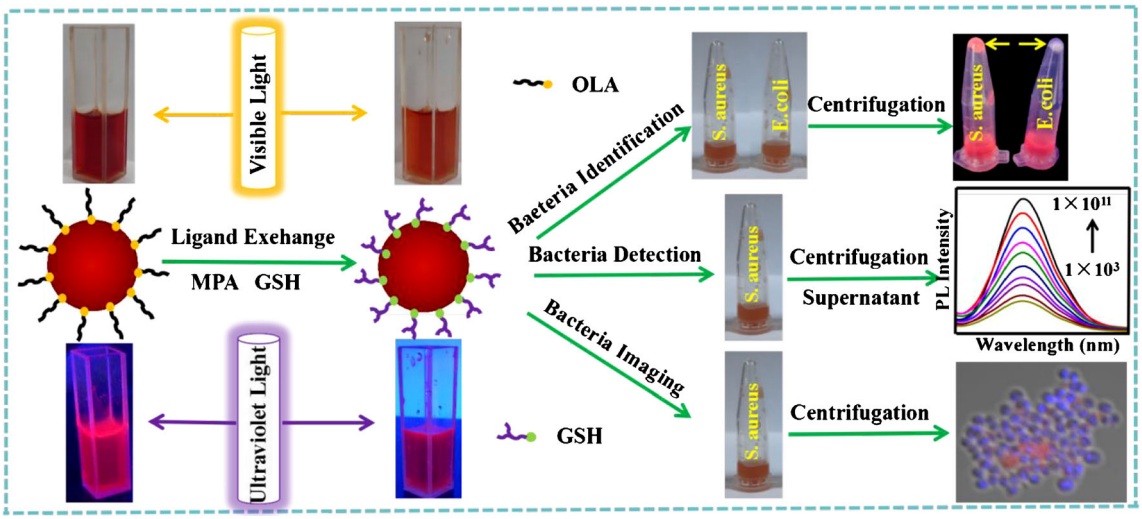

Scheme 1 Schematic illustration of ZnCuInSe QD ligand exchange process and visual discrimination of two bacteria, quantitative detection and imaging of *S. aureus*

solution containing 0.3 mmol of Se powder, 0.1 mL of 1-dodecanethiol, and 1 mL of oleylamine was injected into the flask and the reaction maintained for 20 min. The resulting solution was cooled to room temperature. The as-synthesized QDs were repeatedly purified with ethanol by centrifugation (6000 rpm, 5 min), and the precipitates were dispersed in dichloromethane and stored in a 4 °C refrigerator for further use. The amount of zinc chloride was an experimental variable, at 0, 0.02, 0.05, 0.1, 0.15, and 0.2 mmol.

Aqueous phase transfer using glutathione

A simple and feasible ligand exchange procedure for aqueous phase transfer of oil-solution and color-tunable ZnCuInSe QDs was conducted by using glutathione (GSH) as the ligand. Importantly, hydrophilic ZnCuInSe QDs almost still maintain initial photoluminescence properties, morphology, and crystal structure. Simply, the mixture of 3 mg of GSH, 4mL of 3-mercaptopropionic acid, 1 mL of methanol and 10 mL of oil-soluble ZnCuInSe QDs was added to 3mL *N*,*N*-dimethylformamide in a 50 mL three-neck flask [31]. The mixture was heated to 80 °C under stirring in nitrogen atmosphere. The reaction was quenched when the mixture transitioned from cloudy to clear by placing the flask in an ice water bath. Finally, the resulting solution was centrifuged by addition of excess methanol at 8000 rpm for 10 min. The precipitation separation process was repeated three times, followed by drying under vacuum. Finally, the pure ZnCuInSe QDs were dissolved in deionized water for further use. Moreover, the stability of ZnCuInSe QDs was evaluated by monitoring the photoluminescence after the QDs were stored at 4 °C for a different time.

Bacteria and cell culture

Bacterial strains, including *Staphylococcus aureus* (*S. aureus*), *Bacillus subtilis* (*B. subtilis*), *Escherichia coli* (*E. coli*), and *Acinetobacter baumannii* (*A. baumannii*), were used in the experiments. All kinds of bacteria were sustained in the Luria-Bertani medium. Bacterial cultures were grown 18 h (37 °C, shaking at 150 rpm). Then, bacteria were collected via centrifugation at 8000 rpm for 2 min and washed three times with sterilized saline water, and redispersed in sterilized saline water for further use. Bacterial colony numbers were estimated by the plate counting method. The bacterial solutions were prepared to a serial concentration from 1.0×10 to 1.0×10^{11} CFU/mL for future use. The cells (Hek293T and NIH/3T3) were cultured in Dulbecco's modified Eagle's medium (DMEM) supplemented with 10% (v/v) calf serum, penicillin (100 CFU/mL), and streptomycin (100 mg mL^{-1}) at 37 °C in a humidified atmosphere containing 5% CO_2.

Minimum inhibitory concentration of ZnCuInSe QDs

The inhibitory effects of ZnCuInSe QDs on the growth of bacteria (*S. aureus*, *B. subtilis*, *E. coli*, and *A. baumannii*) were evaluated. The well of a 96-well plate was covered with a mixture of 50 μL Luria-Bertani medium and 50 μL of ZnCuInSe QDs at different concentrations. Then, 100 μL of bacterial supernatant (1×10^5 CFU/mL) was added; hence, the final concentrations of the ZnCuInSe QDs were 2, 4, 8, 16, 32, 64, and 128 μg mL^{-1}, then incubated at 37 °C for 18 h in the dark. Each experiment was performed at least three independent times. The positive control (containing 100 μL Luria-Bertani medium and 100 μL bacterial supernatant) and negative control (200 μL Luria-Bertani medium) were designed as quality controls in this assay. After incubation, the absorbance was measured via a multimodal microplate reader (Synergy 4, BioTek) at 600 nm.

Assay procedure of *S. aureus*

The ZnCuInSe QD (200 μL, 1 mg mL^{-1}) probes were mixed with 200 μL of bacteria at various concentrations (1×10^3–1×10^{11} CFU/mL) and incubated at 37 °C for 30 min under agitation. Thereafter, the solutions were collected by centrifugation at 9000 rpm for 2 min to monitor the photoluminescence intensity. The fluorescence spectra of the obtained solution were measured with a fluorescence spectrophotometer equipped with 450-nm excitation. The intensity differences ($\Delta I = I_0 - I$) between the solution and the control (I_0) were used to generate a standard curve against the logarithm of the bacterial concentration. The 667-nm peak intensity emission wavelength was used. To further evaluate the reliability of the proposed method for practical applications, ZnCuInSe QDs were used to detect *S. aureus* in diluted milk samples. Milk purchased from a local supermarket was diluted 100-fold with 0.9% NaCl. Different concentrations of *S. aureus* solutions were then added to the diluted milk, to which ZnCuInSe QDs were then added.

Biosafety of hydrophilic ZnCuInSe QDs

To evaluate the safety of ZnCuInSe QDs, we used Hek293T cells, NIH/3T3 cells, and red blood cells of sheep for the cytotoxicity experiments. Different concentrations of ZnCuInSe QDs were incubated with aliquots (100 μL) of cells (~ 10^5 cells per mL) in 96-well plates at 37 °C for 24 h. Then, the cells were washed twice before the medium was refreshed. 3-(4,5-Dimethylthiazol-2-yl)-2,5-diphenyltetrazolium bromide was then added, and the absorbance was measured via a multimodal microplate reader at 490 nm after 4-h incubation. We calculate the inhibition rate of cell growth by the formula: cell viability (%) = (mean absorbance value of the treatment group / mean absorbance value of the control) × 100%.

In vitro hemolysis assay was carried out to evaluate hemoglobin (Hb) release in the plasma, an indicator of red blood cell lysis, following ZnCuInSe QD exposure. Typically, 450 μL of 2% red blood cells was mixed with 550 μL ZnCuInSe QDs (at final concentrations of 0.1, 0.3, 0.5, and 1 mg mL^{-1}, respectively) and incubated in a 37 °C water bath for 30 min. The positive control (containing 550 μL water and 450 μL 2% red blood cells) and negative control (containing 550 μL 0.9% NaCl and 450 μL 2% red blood cells) were designed as quality controls. After incubation, red blood cell lysis was pelleted down by centrifugation of the samples at 6000 rpm for 5 min. Then, the optical density (OD) of the supernatant solution was measured at 545 nm. The hemolysis rate was calculated by the formula [32]:

$$\text{hemolysis rate}\ (\%) = \frac{\text{ODpositive-ODnegative}}{\text{ODsample-ODnegative}} \times 100\%,$$

where $OD_{positive}$, $OD_{negative}$, and OD_{sample} represent the absorption values of test, negative, positive, and samples under test.

Confocal images of *S. aureus* and *E. coli*

Fluorescence images were obtained by confocal laser scanning microscopy. In brief, 200 μL of bacterial supernatant was incubated with 200 μL of ZnCuInSe QDs for 1 h, and then centrifuged to remove unbound QDs. The resulting precipitation was re-dispersed in 20 μL 0.9% NaCl solution. Then, 10 μL of DAPI (5 μg mL^{-1}) solution was added and then shaken well, lastly adding 5 μL of the pre-prepared mixed suspensions to clean glass slides and covering them with coverslips for immobilization. The samples were placed in a confocal dish, and fluorescence images of DAPI (λex = 405 nm, λem = 430–500 nm) and ZnCuInSe QDs (λexc = 488 nm, λem = 630–680 nm) were collected.

Apparatus

Absorption spectra of ZnCuInSe QDs were collected using a Cary 60 UV-Vis spectrophotometer (Agilent, USA). A Hitachi F-4600 fluorescence spectrophotometer (Tokyo, Japan) was used to measure photoluminescence (PL) spectra at room temperature with 450-nm excitation wavelength. FTIR spectra were recorded on an IR Affinity-1 spectrophotometer (Shimadzu, Japan). The crystalline phase was analyzed using an X-ray diffractometer (XRD-6100, Shimadzu, Japan) with Cu Kα irradiation source. Transmission electron microscopy (TEM) images of QDs and energy-dispersive spectroscopy (EDS) spectra were acquired on a JEM-2100F microscope (JEOL Ltd.) operating at 200 kV. Bacteria images were obtained with a confocal laser scanning microscope (TI-E+A1 SI, Nikon, Japan).

Results and discussion

Optical properties and structure of the ZnCuInSe QDs

Off-stoichiometric control of the metal element ratio in Zn-doped CIS/Se QDs is one of the key strategies [33] for engineering their PL [34, 35]. Therefore, we changed the zinc content gradually to tune the fluorescence; as shown in Fig. 1a, with the increase of the Zn content from 0 to 0.2 mmol, the PL emission peaks of the ZnCuInSe QDs exhibit a gradual blue shift from 710 to 560 nm, and it can be ascribed to the fact that the band gap of the QDs increases accordingly with the decrease of content of low band gap In_2Se_3 in the $CuInSe_2$ nanoparticles. As the Zn content increases from 0.1 to 0.2 mmol, the absorption band edge of the ZnCuInSe QDs progressively shifts to higher, as shown in Fig. 1b. The QDs with 0.1 mmol zinc chloride have the strongest absorption peak. The inset of Fig. 1b shows the photographs of the ZnCuInSe QDs with different Zn contents in dichloromethane under visible light and 365-nm UV irradiation (down), respectively. Under visible light (up), the color changes from black to red and then to reddish-brown, confirming that the resulting QDs had favorable QYs with the doped Zn element.

To promote application in various biological fields, the ligand exchange process for transfer of hydrophobic ZnCuInSe QDs to hydrophilic ones was performed by using glutathione as the ligand and Fig 1c and d show the PL emission and UV visible absorption spectra of ZnCuInSe QDs with 0.1 mmol zinc content before and after ligand exchange, respectively. The ligand exchange results in the red shift in fluorescence emission peaks and decrease in photoluminescence intensity due to the slight increase in particle size after ligand exchange. Also, there was little change of the absorption spectra after ligand exchange due to the decrease of absolute QY, as shown in the inset of Fig. 1c. The inset of Fig. 1d shows the photographs of the ZnCuInSe QDs before and after ligand exchange under visible light and UV irradiation. The fluorescence color after ligand exchange was not as bright as before ligand exchange, but the bright fluorescence was still observed clearly under the 365-nm UV irradiation.

The FTIR spectra of QDs were compared with those of before and after ligand exchange, as shown in Fig. 1e. The peak at 3350 cm^{-1} corresponds to the –NH stretching of oleylamine-covered hydrophobic ZnCuInSe QDs, which disappears after ligand exchange. Also, the peak at 1701 cm^{-1} for hydrophilic ZnCuInSe QDs corresponds to the >C=O group of –COOH in glutathione. The FTIR spectrum confirms capping of glutathione on ZnCuInSe QDs. No –SH stretching vibration was observed at 2557 cm^{-1} after ligand exchange because the glutathione covered the surface of ZnCuInSe QDs via the s–Cu chemical bond after cleavage of the S–H bond [36].

Moreover, the stability of ZnCuInSe QDs was evaluated by monitoring the photoluminescence after the QDs were stored at 4 °C for a different time, as shown in Fig. 1f. The

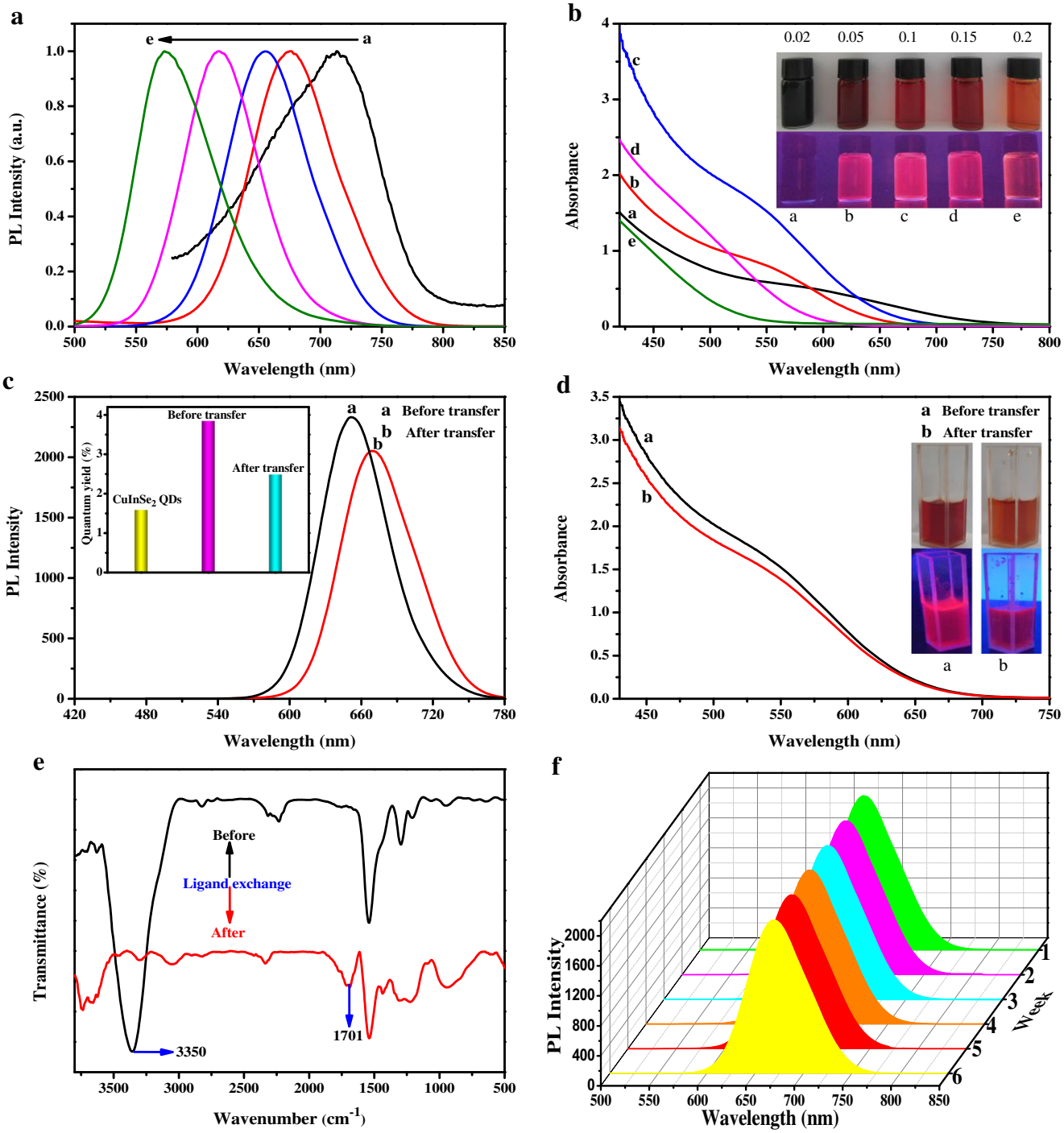

Fig. 1 Fluorescence and absorption spectra of ZnCuInSe QDs with different Zn contents (**a** and **b**), before and after ligand exchange with 0.1 mmol Zn content (**c** and **d**). The insets of panel show the digital photographs of ZnCuInSe QDs with different Zn contents (**b**), before and after ligand exchange with 0.1 mmol Zn content (**d**) under visible light and UV light (365 nm), and the QY of the QDs before and after doping Zn element and hydrophilic ZnCuInSe QDs (**c**). (**e**) FTIR spectra of ZnCuInSe QDs before and after ligand exchange. (**f**) The photoluminescence of the ZnCuInSe QDs for different stored time periods

photoluminescence intensity and wavelength were observed without a salient decrease, indicating excellent long-term storage stability of ZnCuInSe QDs.

QD crystal structures were determined by wide-angle XRD, as shown in Fig. 2a. The patterns for QD samples with zinc contents of 0, 0.02, 0.05, 0.1, 0.15, and 0.2 mmol and hydrophilic ZnCuInSe QDs exhibit characteristic diffraction patterns for a chalcopyrite structure (JCPDS: No. 40-1487). There are two diffraction peaks around 2θ values of 27.1° and 44° for $CuInSe_2$ QDs,

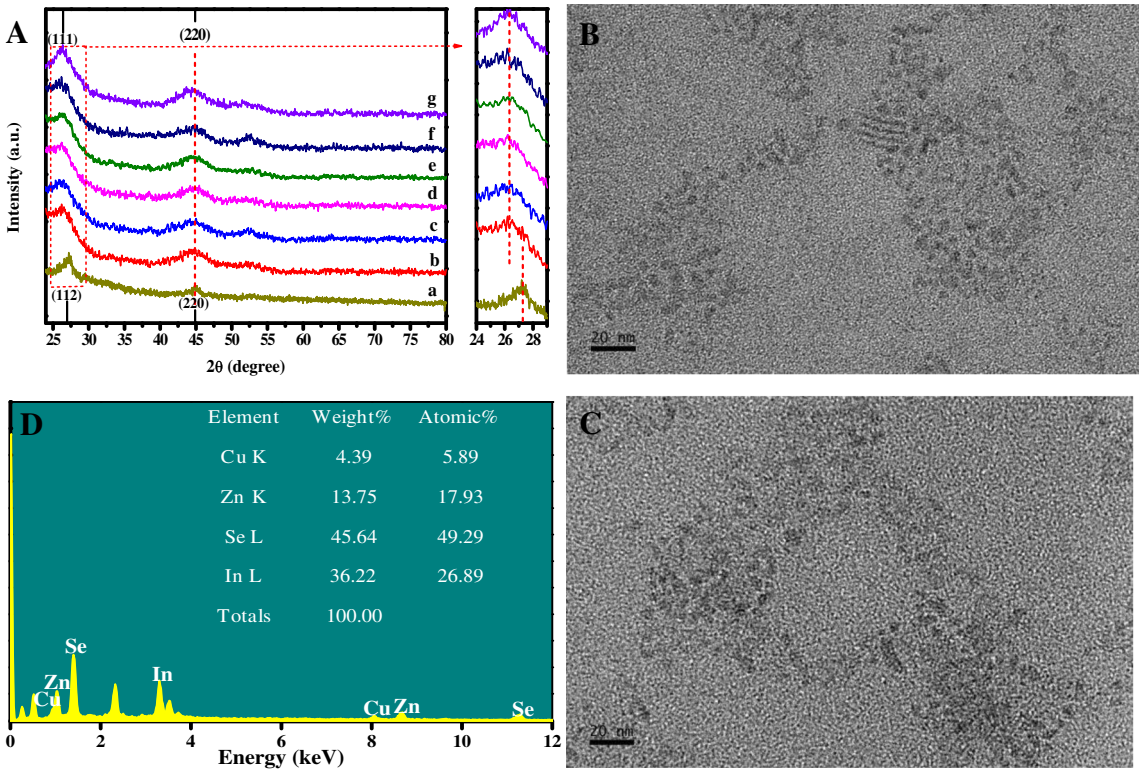

Fig. 2 (**A**) XRD pattern with zinc contents of 0, 0.02, 0.05, 0.1, 0.15, and 0.2 mmol and hydrophilic ZnCuInSe QDs (**a**–**g**); TEM image of ZnCuInSe QDs before (**B**) and after (**C**) ligand exchange with 0.1 mmol zinc. (**D**) The EDX spectrum of ZnCuInSe QDs after ligand exchange

corresponding to the (112) and (220) phases of the chalcopyrite structure. With addition of zinc, the peak positions shifted steadily from chalcopyrite $CuInSe_2$ to zinc blend ZnSe, indicating the formation of doped QDs [37]. However, there is no obvious change in the excitonic peak positions with the increase of zinc content, possibly due to the small change in the content of zinc. The peak positions for the samples before and after ligand exchange are almost the same, indicating no obvious change in the structure.

Figure 2b and c present the TEM images of the ZnCuInSe QDs before and after ligand exchange. It appears that the QDs are well isolated and rarely observed as aggregates, which evidenced the good dispersity. The favorable dispersibility satisfies the request for general biological imaging application. However, the size of the hydrophilic ZnCuInSe QDs slightly increased after ligand exchange, which may be the reason for the emission wavelength red shift. The EDS spectrum of hydrophilic ZnCuInSe QDs reveals the characteristic peaks of Zn, Cu, In, and Se element (see Fig. 2d).

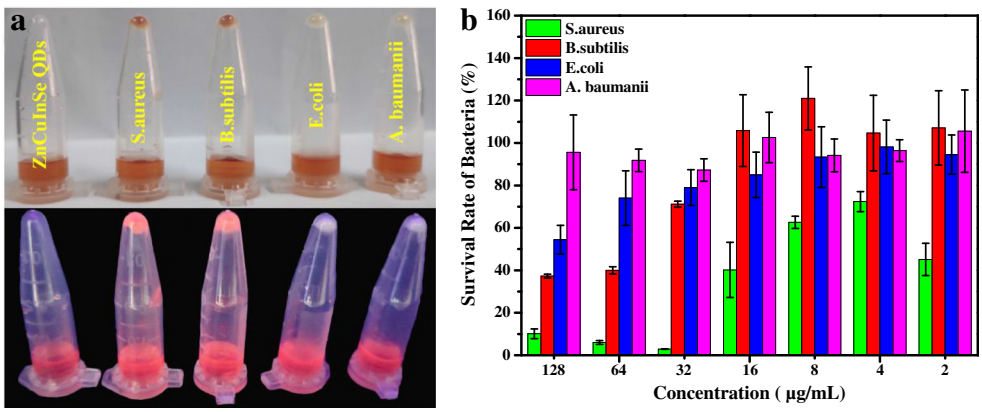

Fig. 3 (**a**) Digital photographs of ZnCuInSe QDs and bacteria incubation after centrifugation. (**b**) Inhibitory effects of different concentrations of ZnCuInSe QDs on four bacteria

ZnCuInSe QDs–based rapid classification of Gram-positive/Gram-negative bacteria and minimal inhibitory concentration test

The interaction of ZnCuInSe QDs with Gram-positive or Gram-negative bacteria is determined by the bacterial surface characteristics. Gram-positive bacteria only have a cytoplasmic membrane covered by a loose and poriferous cell wall. In contrast, Gram-negative bacteria possess an additional outer membrane, which exerts the barrier function. The difference in surface structures of the two types of bacteria determines whether ZnCuInSe QDs can be combined with them. In this work, we selected two Gram-positive (*S. aureus* and *B. subtilis*) and two Gram-negative (*E. coli* and *A. baumannii*) bacteria for research. Briefly, hydrophilic ZnCuInSe QDs were incubated with these bacteria for 30 min, respectively,

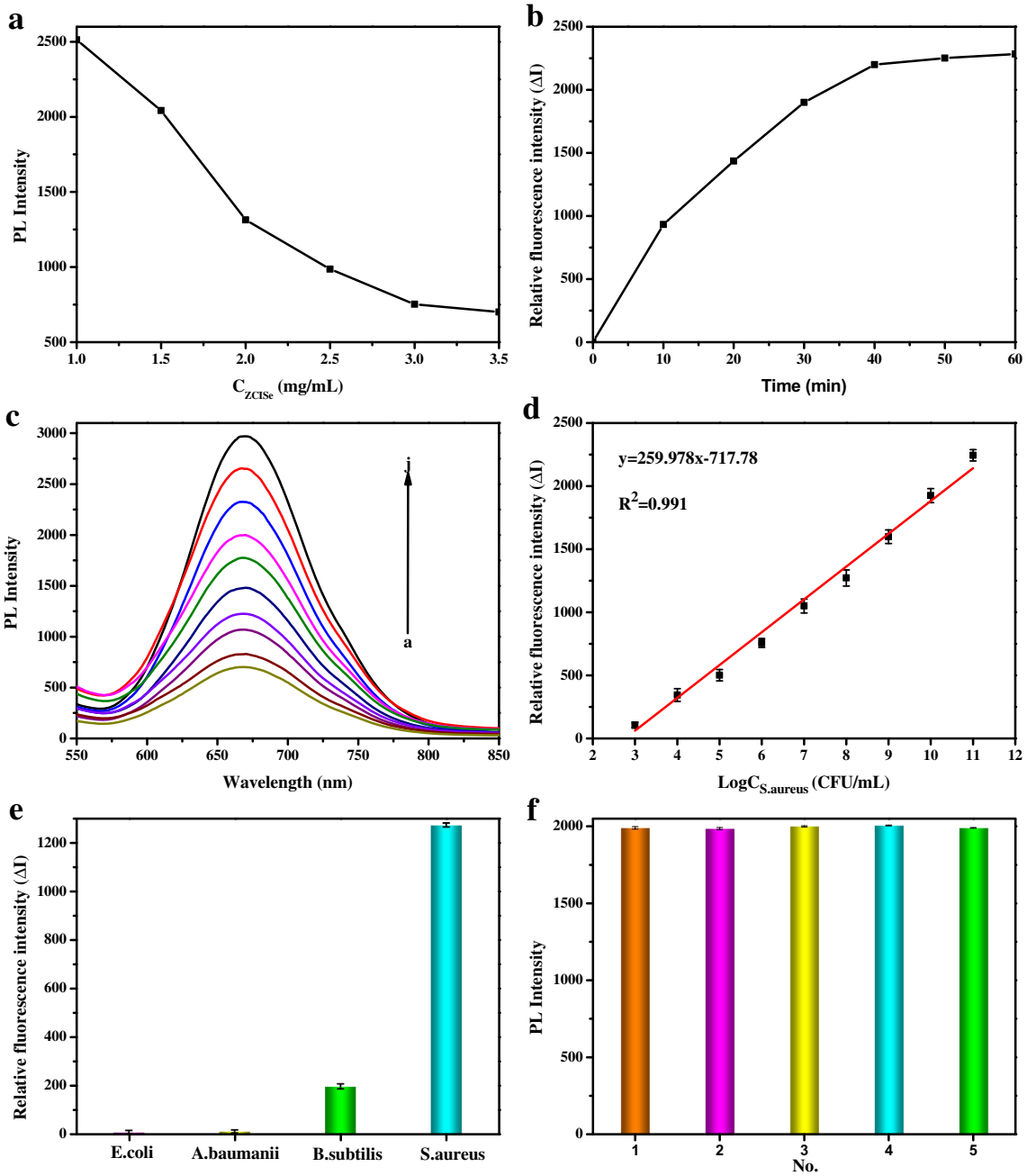

Fig. 4 (**a**) The fluorescence intensity of ZnCuInSe QDs at different concentrations. (**b**) The variation of relative intensity with the incubation time of ZnCuInSe QDs with bacteria. (**c**) Fluorescence spectra of ZnCuInSe QDs at different *S. aureus* concentrations (**a**, 0 CFU/mL; **b**–**j**, 1×10^3–1×10^{11} CFU/mL). (**d**) Plot of fluorescence intensity at 667 nm against the log of *S. aureus* concentration. (**e**) Fluorescence responses of the hydrophilic ZnCuInSe QDs to four bacteria at 1×10^8 CFU/mL. (**f**) The reproducibility of the analytical performance by detecting 1×10^8 CFU/mL *S. aureus*

Table 1 Detection of *S. aureus* in milk samples with ZnCuInSe QDs

Sample	Blank	Added *S. aureus* (CFU/mL)	Found *S. aureus* (CFU/mL)	Recovery (%)
1	0	1×10^3	1.083×10^3	108.3
2	0	1×10^4	9.962×10^3	99.61
3	0	1×10^5	9.937×10^4	99.37
4	0	1×10^6	1.045×10^6	104.5

and then centrifuged to obtain the precipitate. As shown in Fig. 3a, a distinct red color at the bottom of the centrifuge tube was observed for *S. aureus* and *B. subtilis*, but not for *E. coli* and *A. baumannii*. The obvious binding effect of QDs with Gram-positive bacteria suggests the potential of developing a simple method for rapid classification of the two types of bacteria.

We further conducted the minimal inhibitory concentration assay for these four kinds of bacteria. Figure 3b shows that the inhibition effect of ZnCuInSe QDs on the growth of Gram-positive bacteria, especially *S. aureus*, is more obvious than that of other bacteria.

Detection of *S. aureus*

We first measured the photoluminescence intensity of ZnCuInSe QDs at different concentrations, as shown in Fig. 4a; the intensity decreases with the increase of concentration from 1 to 3 mg mL^{-1}, after which the intensity is unchanged, which was caused by the concentration quenching effect: QDs have a wide absorption band. When the concentration of QDs reaches a certain value, the QDs cannot be excited completely by the incident light, so the stimulated QDs do not increase. However, the increase of absorption causes the fluorescence intensity to weaken. Therefore, the optimal concentration of ZnCuInSe QDs was set as 3 mg mL^{-1}. Figure 4b shows the relative intensity increase with incubation time from 0 to 40 min. Therefore, 40 min was chosen as the optimal incubation time in subsequent experiments.

In the absence of *S. aureus*, the fluorescence intensity of the ZnCuInSe QDs is of minimal value. After adding *S. aureus* for incubation and centrifugation, some of the QDs co-precipitate with the *S. aureus* due to their binding, and the QDs in the solution are reduced; hence, the fluorescence intensity of ZnCuInSe QDs in the solution is dramatically enhanced. Figure 4c shows the *S. aureus* concentration–dependent fluorescence intensity, and as the concentration of *S. aureus* increases from 1×10^3 to 1×10^{11} CFU/mL, the fluorescence intensity of ZnCuInSe QDs in supernatant at the wavelength of 667 nm is gradually enhanced. Good linearity between the difference of the fluorescence intensity of ZnCuInSe QDs in supernatant and *S. aureus* concentration in the concentration range of 1×10^3–1×10^{11} CFU/mL is obtained (see Fig. 4d). The linear regression equation was $\Delta I = 259.978 \log C_{S.\ aureus} - 717.78$, with a correlation coefficient of 0.991. The limit of detection is defined as the lowest concentration that can be detected; in this work, the LOD was 1×10^3 CFU/mL.

To evaluate the specificity of the ZnCuInSe QDs, the QD responses to four bacteria were measured, as shown in Fig. 4e, and the QDs exhibit little responses to *B. subtilis*, *E. coli*, and *A. baumannii*, indicating a high specificity of the ZnCuInSe QDs towards *S. aureus*.

The reproducibility and the stability of the analytical performance were investigated by detecting 1.0×10^8 CFU/mL *S. aureus* with five ZnCuInSe QDs prepared independently under identical conditions, as shown in Fig. 4f. The results indicate that the ZnCuInSe QDs have a good reproducibility and stability for the detection of *S. aureus*.

To evaluate the utility of ZnCuInSe QDs in real samples, different concentrations of *S. aureus* were artificially added to milk samples. As shown in Table 1, the average recovery is 102.945%, indicating that ZnCuInSe QDs can be applied to the detection of bacteria in actual samples.

Various detection methods have been reported for quantitative detection of bacteria. Several fluorescence-based

Table 2 Other fluorescence-based detection methods

Fluorescent material	Modified material	LOD (CFU mL^{-1})	Linear range	Reference
CdTe/CdS QDs	Antibodies	10^4	_	[22]
CdSe/ZnS QDs	Immune magnetic	14	8.9–8.9×10^5	[21]
Si NPs	Aptamer	150	_	[38]
QDs/DNA	Antibodies	1.37	1.0–1.0×10^8	[19]
Si NPs	Dielectrophoresis	270	_	[39]
ZnCuInSe QDs	_	10^3	1.0×10^3–1.0×10^{11}	This work

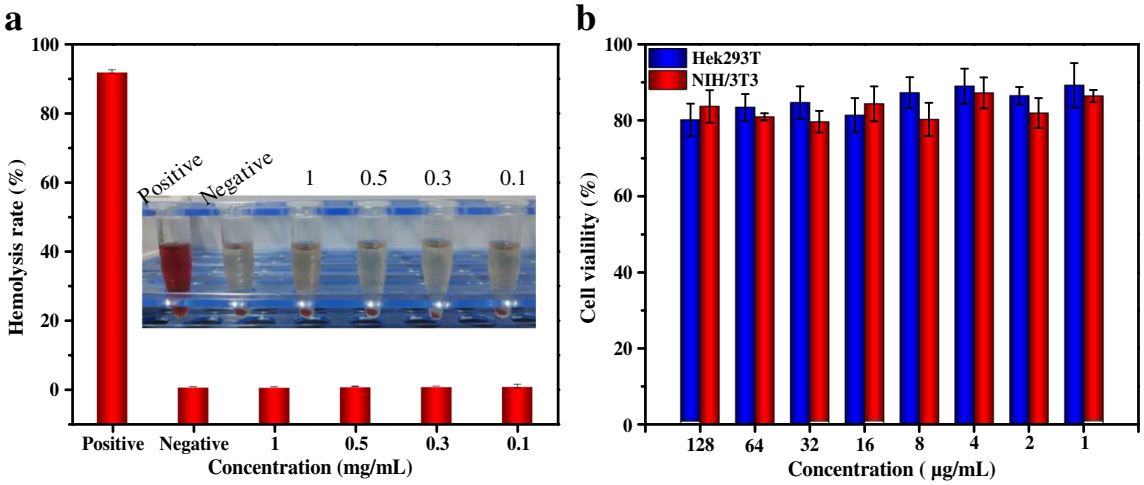

Fig. 5 Biosafety of the hydrophilic ZnCuInSe QDs. The blood (**a**), and the Hek293T cell and NIH/3T3 cell (**b**) compatibility

detection methods are summarized in Table 2 [38, 39]. Compared with the reported methods, our detection method avoids heavy metal elements, requires no complex surface modifications, and possesses a wide detection range. The total detection time from the addition of the ZnCuInSe QDs to the *S. aureus* solution to obtaining the final result was less than 1 h.

Biocompatibility and imaging applications of hydrophilic ZnCuInSe QDs

As shown in Fig. 5a, the hemolysis rate of hydrophilic ZnCuInSe QDs is far below the hemolysis rate threshold value of 5%. Using the MTT method, the cell viability of both the Hek293T and NIH/3T3 cells at 128 μg mL^{-1} QDs remained at more than 80%, indicating that the ZnCuInSe QDs own excellent biocompatibility and could be safely used in imaging (see Fig. 5b). It is worth noting that ZnCuInSe QDs show inhibiting effect to bacteria but not cells at the same concentration, and this is caused by their different structures.

As shown in Fig. 6, fluorescence images of DAPI (blue) and ZnCuInSe QDs (red) were clearly observed in *S. aureus*, indicating the potential for further application of the QDs in bioimaging and diagnosis. With *E. coli*, we only found the fluorescence images of DAPI (blue) and no ZnCuInSe QDs (red), confirming the selectivity of QDs for Gram-positive bacteria—the result consistent with the result shown in Fig. 3a.

Conclusions

Aqueous phase transfer of ZnCuInSe QDs was achieved through an efficient ligand exchange strategy using GSH as the bifunctional ligand. The hydrophilic ZnCuInSe QDs can rapidly classify Gram-positive and Gram-negative bacteria according to their different binding forces. The ZnCuInSe

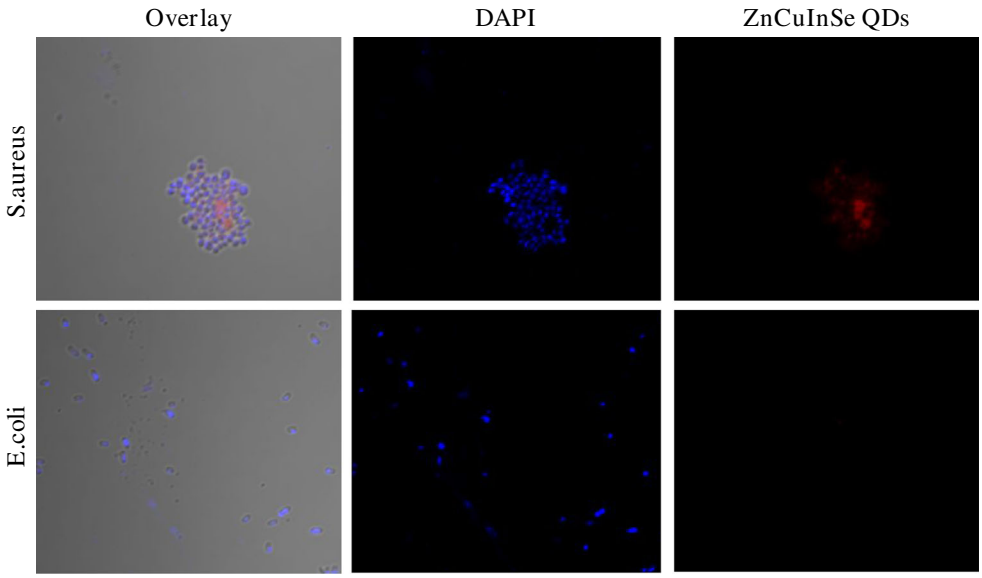

Fig. 6 Confocal fluorescence images of samples incubated with *S. aureus* and *E. coli*

QDs can detect *S. aureus* as low as 1×10^3 CFU/mL within 45 min and show excellent linear relationship in the range of 1×10^3 to 1×10^{11} CFU mL^{-1}. The small particle size and good fluorescence intensity make ZnCuInSe QDs promising candidates for optical bioimaging. Our work suggests ZnCuInSe QDs can be used as a low toxicity and technically simple biological probe, providing a convenient, sensitive, and stable platform for biological applications.

Funding We gratefully acknowledge the National Natural Science Foundation of China (Grant Nos. 21874038, 21605090) for financial support.

Compliance with ethical standards

Conflict of interest The authors declare that they have no conflict of interest.

References

1. Salwiczek M, Qu Y, Gardiner J, Strugnell RA, Lithgow T, McLean KM, et al. Emerging rules for effective antimicrobial coatings. Trends Biotechnol. 2014;32:82–90.
2. Chen J, Andler SM, Goddard JM, Nugen SR, Rotello VM. Integrating recognition elements with nanomaterials for bacteria sensing. Chem Soc Rev. 2017;46:1272–83.
3. Kwon HY, Liu X, Choi EG, Lee JY, Choi SY, Kim JY, et al. Development of a universal fluorescent probe for Gram-positive bacteria. Angew Chem Int Edit. 2019;58:8426–31.
4. Kim JH, Grant SB. Public mis-notification of coastal water quality: a probabilistic evaluation of posting errors at Huntington Beach, California. Environ Sci Technol. 2004;38:2497–504.
5. Maalouf R, Fournier WC, Coste J, Chebib H, Saïkali Y, Vittori O, et al. Label-free detection of bacteria by electrochemical impedance spectroscopy: comparison to surface plasmon resonance. Anal Chem. 2007;79(13):4879–86.
6. Lisalova VH, Visova I, Ermini ML, Springer T, Song XC, Mrazek J, et al. Low-fouling surface plasmon resonance biosensor for multi-step detection of foodborne bacterial pathogens in complex food samples. Biosens Bioelectron. 2016;80:84–90.
7. Wang YX, Ye ZZ, Si CY, Ying YB. Monitoring of Escherichia coli O157:H7 in food samples using lectin based surface plasmon resonance biosensor. Food Chem. 2013;136(3–4):1303–8.
8. Gao WC, Li B, Yao RZ, Li ZP, Wang XW, Dong XL, et al. Intuitive label-free SERS detection of bacteria using aptamer-based in situ silver nanoparticles synthesis. Anal Chem. 2017;89(18):9836–42.
9. Preciado-Flores S, Wheeler DA, Tran TM, Tanaka Z, Jiang C, Barboza-Flores M, et al. SERS spectroscopy and SERS imaging of Shewanella oneidensis using silver nanoparticles and nanowires. Chem Commun. 2011;47(14):4129–31.
10. Yang X, Gu C, Qian F, Li Y, Zhang JZ. Highly sensitive detection of proteins and bacteria in aqueous solution using surface-enhanced Raman scattering and optical fibers. Anal Chem. 2011;83(15):5888–94.
11. Tamminen M, Joutsjoki T, Sjoblom M, Joutsen M, Palva A, Ryhanen EL, et al. Screening of lactic acid bacteria from fermented vegetables by carbohydrate profiling and PCR-ELISA. Lett Appl Microbiol. 2004;39(5):439–44.
12. Chen R, Huang XL, Xu HY, Xiong YH, Li YB. Plasmonic enzyme-linked immunosorbent assay using nanospherical brushes as a catalase container for colorimetric detection of ultralow concentrations of Listeria monocytogenes. ACS Appl Mater Interfaces. 2015;7(51):28632–9.
13. Zhu YD, Gasilova N, Jovic M, Qiao L, Liu BH, Lovey LT, et al. Detection of antimicrobial resistance-associated proteins by titanium dioxide-facilitated intact bacteria mass spectrometry. Chem Sci. 2018;9(8):2212–21.
14. Steil D, Pohlentz G, Legros N, Mormann M, Mellmann A, Karch H, et al. Combining mass spectrometry, surface acoustic wave interaction analysis, and cell viability assays for characterization of Shiga toxin subtypes of pathogenic Escherichia coli bacteria. Anal Chem. 2018;90(15):8989–97.
15. Yin BF, Wang Y, Dong ML, Wu J, Ran B, Xie MX, et al. One-step multiplexed detection of foodborne pathogens: combining a quantum dot-mediated reverse assaying strategy and magnetic separation. Biosens Bioelectron. 2016;86:996–1002.
16. Sapsford KE, Rasooly A, Taitt CR, Ligler FS. Detection of Campylobacter and Shigella species in food samples using an array biosensor. Anal Chem. 2004;76:433–40.
17. Guo PL, Tang M, Hong SL, Yu X, Pang DW, Zhang ZL. Combination of dynamic magnetophoretic separation and stationary magnetic trap for highly sensitive and selective detection of Salmonella typhimurium in complex matrix. Biosens Bioelectron. 2015;74:628–36.
18. Ma Q, Nakane Y, Mori Y, Hasegawa M, et al. Multilayered, core/shell nanoprobes based on magnetic ferric oxide particles and quantum dots for multimodality imaging of breast cancer tumors. Biomaterials. 2012;33(33):8486–94.
19. Wen JL, Zhou SG, Yu Z, Chen JH, Yang GQ, Tang J. Decomposable quantum-dots/DNA nanosphere for rapid and ultrasensitive detection of extracellular respiring bacteria. Biosens Bioelectron. 2018;100:469–74.
20. Dogan Ü, Kasap E, Cetin D, Suludere Z, Boyaci IH, Türkyılmaz C, et al. Rapid detection of bacteria based on homogenous immunoassay using chitosan modified quantum dots. Sensors Actuators B Chem. 2016;233:369–78.
21. Xue L, Zheng LY, Zhang HL, Jin X, Lin JN. An ultrasensitive fluorescent biosensor using high gradient magnetic separation and quantum dots for fast detection of foodborne pathogenic bacteria. Sensors Actuators B Chem. 2018;265:318–25.
22. Yu JL, Su J, Zhang J, Wei XT, Guo AL. CdTe/CdS quantum dot-labeled fluorescent immunochromatography test strips for rapid detection of Escherichia coli O157:H7. RSC Adv. 2017;7(29):17819–23.
23. Booth M, Brown AP, Evans SD, Critchley K. Determining the concentration of $CuInS_2$ quantum dots from the size-dependent molar extinction coefficient. Chem Mater. 2012;24(11):2064–70.
24. Leach AD, Macdonald JE. Optoelectronic properties of $CuInS_2$ nanocrystals and their origin. J Phys Chem Lett. 2016;7(3):572–83.
25. Park J, Dvoracek C, Lee KH, Galloway JF, Bhang HE, Pomper MG, et al. CuInSe/ZnS core/shell NIR quantum dots for biomedical imaging. Small. 2011;7(22):3148–52.
26. Nose K, Omata T. Colloidal synthesis of ternary copper indium diselenide quantum dots and their optical properties. J Phys Chem C. 2009;113:3455–60.
27. Allen PM, Bawendi MG. Ternary I-III-VI quantum dots luminescent in the red to near-infrared. J Am Chem Soc. 2008;130:9240–1.
28. Zhang R, Deng T, Wang J, Wu G, Li SR, Gu YQ, et al. Organic-to-aqueous phase transfer of Zn–Cu–In–Se/ZnS quantum dots with multifunctional multidentate polymer ligands for biomedical optical imaging. New J Chem. 2017;41(13):5387–94.
29. Pons T, Bouccara S, Loriette V, Lequeux N, Pezet S, Fragola A. In vivo imaging of single tumor cells in fast-flowing bloodstream using near-infrared quantum dots and time-gated imaging. ACS Nano. 2019;13(3):3125–31.

30. Li WL, Geng HC, Yao L, Cao KS, Sheng PT, Cai QY. Photoelectrocatalytic hydrogen generation enabled by CdS passivated ZnCuInSe quantum dot-sensitized TiO_2 decorated with Ag nanoparticles. Nanomaterials. 2019;9(3):393.
31. Yao L, Geng HC, Cheng RR, Cao KS, Sheng PT, Li WL, et al. Preparation of hybrid photoelectrode based on defect-poor Zn-$CuInSe_2$ QDs sensitized nanoporous ZnO nanosheets with an application in azo dye removal. J Mater Sci Mater Electron. 2019;30(8):7928–39.
32. Liu K, Yan X, Xu YJ, Dong L, Hao LN, Song YH, et al. Sequential growth of CaF_2:Yb,Er@CaF_2:Gd nanoparticles for efficient magnetic resonance angiography and tumor diagnosis. Biomater Sci. 2017;5(12):2403–15.
33. Zhang WJ, Lou Q, Ji WY, Zhao JL, Zhong XH. Color-tunable highly bright photoluminescence of cadmium-free Cu-doped Zn-In-S nanocrystals and electroluminescence. Chem Mater. 2014;26(2):1204–12.
34. Zhang BT, Wang YC, Yang CB, Hu SY, Gao Y, Zhang YP, et al. The composition effect on the optical properties of aqueous synthesized Cu–In–S and Zn–Cu–In–S quantum dot nanocrystals. Phys Chem Chem Phys. 2015;17(38):25133–41.
35. Xu YQ, Chen T, Hu XB, Jiang W, Wang LJ, Jiang WH, et al. The off-stoichiometry effect on the optical properties of water-soluble copper indium zinc sulfide quantum dots. J Colloid Interface Sci. 2017;496:479–86.
36. Chen XF, Guo ZZ, Miao P. One-pot synthesis of GSH-capped CdTe quantum dots with excellent biocompatibility for direct cell imaging. Heliyon. 2018;4(3):e00576. https://doi.org/10.1016/j.heliyon.2018.e00576.
37. Du J, Du ZL, Hu JS, Pan ZX, Shen Q, Sun JK, et al. Zn-Cu-In-Se quantum dot solar cells with a certified power conversion efficiency of 11.6%. J Am Chem Soc. 2016;138(12):4201–9.
38. He XX, Li YH, He DG, Wang KM, Shangguan JF, Shi H. Aptamer-fluorescent silica nanoparticles bioconjugates based dual-color flow cytometry for specific detection of Staphylococcus aureus. J Biomed Nanotechnol. 2014;10(7):1359–68.
39. Shangguan JF, Li YH, He DG, He XX, Wang KM, Zou Z, et al. A combination of positive dielectrophoresis driven on-line enrichment and aptamer-fluorescent silica nanoparticle label for rapid and sensitive detection of Staphylococcus aureus. Analyst. 2015;140:4489–97.